Tellus (1998), 50B, 491–505
Printed in UK – all rights reserved

TELLUS
ISSN 0280–6509

Uncertainties in assessing radiative forcing by mineral dust

By T. CLAQUIN[1,2]*, M. SCHULZ[1], Y. BALKANSKI[2] and O. BOUCHER[3], [1]*Institut für Anorganische und Angewandte Chemie, Universität Hamburg, Germany;* [2]*Laboratoire des Sciences du Climat et de l'Environnement, CEA-CNRS, Saclay, France;* [3]*Laboratoire d'Optique Atmosphérique, Université de Lille 1, France*

(Manuscript received 4 March 1998; in final form 18 June 1998)

ABSTRACT

The assessment of the climatic effects of an aerosol with a large variability like mineral dust requires some approximations whose validity is investigated in this paper. Calculations of direct radiative forcing by mineral dust (short-wave, long-wave and net) are performed with a single-column radiation model for two standard cases in clear sky condition: a desert case and an oceanic case. Surface forcing result from a large diminution of the short-wave fluxes and of the increase in down-welling long-wave fluxes. Top of the atmosphere (TOA) forcing is negative when short-wave backscattering dominates, for instance above the ocean, and positive when short-wave or long-wave absorption dominates, which occurs above deserts. We study here the sensitivity of these mineral forcings to different treatments of the aerosol complex refractive index and size distribution. We also describe the importance of the dust vertical profile, ground temperature, emissivity and albedo. Among these parameters, the aerosol complex refractive index has been identified as a critical parameter given the paucity and the incertitude associated with it. Furthermore, the imaginary part of the refractive index is inadequate if spectrally averaged. Its natural variability (linked to mineralogical characteristics) lead to variations of up to $\pm 40\%$ in aerosol forcing calculations. A proper representation of the size distribution when modelling mineral aerosols is required since dust optical properties are very sensitive to the presence of small particles. In addition we demonstrate that LW forcing imply a non-negligible sensitivity to the vertical profiles of temperature and dust, the latter being an important constraint for dust effect calculations.

1. Introduction

Aerosol particles are known to affect the radiation balance of the Earth through scattering, absorption, and emission of radiation (the direct effect) and because they can act as cloud condensation nuclei, thereby modifying cloud albedo and lifetime (the indirect effect, Twomey et al., 1984). There is a growing body of evidences that aerosols are responsible for a significant climate forcing since the pre-industrial times although the magnitude of these effects is very uncertain (IPCC, 1995). Aerosol concentration and composition vary widely from region to region because aerosol sources are very different. Anthropogenic activities produce sulfate, nitrate, soot, and organic particles, biomass burning is responsible for smoke (composed of soot and organics), whereas mineral dust outpours downwind the main arid and semi-arid regions of the Earth. The direct short-wave effect of sulfate has been estimated within the range -0.3 to -1 W m^{-2} (Charlson et al., 1992, Kiehl and Briegleb, 1993, Boucher and Anderson, 1995). Penner et al. (1992) showed that biomass burning has an effect of similar magnitude and same sign. Estimation of the radiative forcing by mineral dust is complicated by additional factors. First and in contrast to "pure" sulfate particles, absorption of solar radiation and effect on long-wave radiation (greenhouse effect) have to be

* Corresponding author.

considered. Second, the large space and time variability of aerosol concentration and composition requires that calculations be accurate for a large range of aerosol optical depths and particle sizes. Third, we need a good description of local parameters, such as surface short-wave albedo, R_s, and long-wave emissivity, ε, as well as surface and atmospheric temperatures.

The knowledge of aerosol parameters (distribution and composition) and radiative fluxes is provided by *in-situ* measurements (Fouquart et al., 1987; Ackermann and Chung, 1992) with limited coverage. Satellite instruments (such as Meteostat, AVHRR (Advanced Very High Resolution Radiometer) or POLDER) can provide estimates of dust optical depth over ocean surfaces devoid of clouds (Tanré et al., 1988; Dulac et al., 1992; Husar and Stowe, 1997), but particle non-sphericity, accuracy of aerosol model and discrimination between cloudy and dusty pixels are clearly an issue. The use of modelling therefore appears to be necessary to provide a global coverage of dust geographical and altitude distribution that satellite are not able to provide yet. Global simulations of the mineral dust transport and radiative impact have been initiated by Tegen et al. (1996) and Tegen and Lacis (1996). They concluded to an average 1 W m^{-2} loss of radiation at the surface but found a small change in flux at the top of the atmosphere (TOA). To facilitate such a calculation on a global scale, Tegen and Lacis (1996) resorted to discretisize the size distribution in 8 bins and chose a constant refractive index. However, measurements of this refractive index show large scatter (Sokolik et al., 1993), which might pose problems for a precise description of the dynamics of optical properties.

The scope of this paper is to outline some critical points in the global modelling of dust climatic impact. We investigate the sensitivity of its forcing (SW, LW and net — TOA and surface) to a set of critical parameters like aerosol size distribution, refractive index and atmospheric column properties. The accuracy of the above-mentioned parameters needed to achieve a realistic dust forcing is determined from the sensitivity tests.

2. Model and method

The evaluation of dust radiative effect require a global dust distribution, but results of transport models still need to be refined, especially downwind of Asian and south Hemispheric sources. We assume then that this sensitivity study can be done with a one dimensional radiative code and two cases representative of dust natural variability. Having in mind that the Atlantic plume extending from the Sahara well out to America may be the most important region when considering mineral dust effects and variability, we take the two standard cases along this plume. The desert case, above the Sahara, is chosen because the largest dust concentrations and particles with large radii occur there, having potentially a large radiative impact. The ocean case represents the globally largest uniform surface over which dust can be encountered and accounts for a background dust effect far from the source. Other situations of interest can be inferred from tables and figures. It is nowadays impossible to distinguish natural from human-influenced dust, especially because the knowledge of the historical evolution of dust sources is poor. Representative values for each parameter in the two cases are therefore chosen according to present-time observations.

2.1. Atmospheric properties

Our set of parameters for the desert and the oceanic cases are described in Table 1. According to the literature, surface SW albedo, R_s, is 0.3 over the desert (Cabot, 1995) and 0.06 over the ocean (Payne, 1972), and the LW surface emissivity, ε, is 1 (Legrand et al., 1992). We do not account for spectral dependence in R_s or ε. We took a mean annual surface temperatures T_{surf} of 27 and 24°C over the desert and the ocean, respectively. The seasonal variation of these temperatures was introduced by a sinusoidal adjustment. The diurnal amplitude of surface temperature is 30°C over the desert (Legrand et al., 1992) and is neglected over the ocean. This diurnal variation in temperature is attenuated with height over desert and vanishes at the top of the boundary layer (Riehl, 1954). We represent in Fig. 1 the temperature decrease with height over the desert and a temperature inversion between 980 and 900 hPa over the ocean (Carlson and Benjamin, 1980).

2.2. Aerosol properties

Particles are distributed following a log-normal function:

$$n(r) = \frac{N_0}{\sqrt{2\pi} r \sigma_0} \exp\left(\frac{-(\ln r - \ln mnr)^2}{2\sigma_0^2}\right), \qquad (1)$$

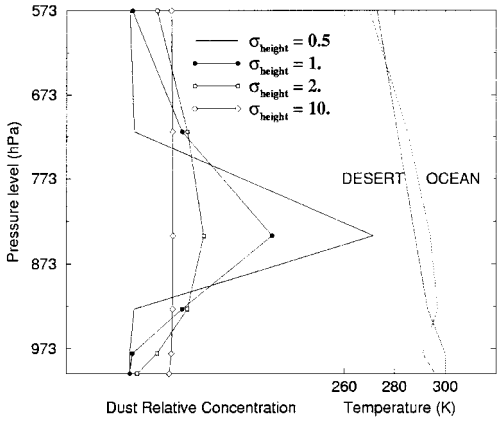

Fig. 1. Dust vertical distributions simulated with the normal distribution (see text) for different values of σ_{height}. Concentrations are given in relative unit since the distributions are normalised to a same total optical depth τ_0 between the surface and 573 hPa. Vertical profiles of temperature are also given for the two standard cases (desert and oceanic with inversion).

where $n(r)\,\mathrm{d}r$ is the number of particle radius between r and $r+\mathrm{d}r$, $\sigma_0 = \ln \sigma_g$ the standard deviation, σ_g being the geometric standard deviation, *mnr* the mean number radius, and N_0 the total number of particles. Such a distribution is adequate for mineral dust (Gomes et al., 1990). We consider a size distribution of mineral dust with $\sigma_g = 2$ and $mnr = 0.7$ μm ($mmr = 2.95$ μm) in the desert (d'Almeida, 1987) and 0.2 μm ($mmr =$ 0.84 μm) over the ocean (Schütz, 1979). Associated to the refractive indices described later, these distributions produce Angström coefficients of -0.09 (ocean case) and -0.15 (desert case), which are realistic for pure dust cloud (Schütz, 1980; Dulac, 1992; Chiapello, personal communication). Gomes et al. (1990) showed that a submicron mode sometimes appears in aerosol source regions, but to facilitate comparisons in this sensitivity study, we will only consider one mode in the desert case.

The distribution of dust optical depth with height is idealised following a normal distribution:

$$\tau(p) = \frac{\tau_0 \exp\left(\dfrac{-(p-p_0)^2}{2\sigma_{\text{height}}^2}\right)}{\displaystyle\int_{1013\,\text{hPa}}^{573\,\text{hPa}} \exp\left(\frac{-(p-p_0)^2}{2\sigma_{\text{height}}^2}\right) \mathrm{d}p}, \qquad (2)$$

where p is pressure, σ_{height} the standard deviation, τ_0 the aerosol optical depth and p_0 the mean pressure of the dust cloud. The distribution is normalised so that the integrated optical depth between the ground and 573 hPa is τ_0. The dust vertical distribution is presented in Fig. 1. We use the 11 levels vertical resolution of typical global models (GCM or chemical transport model). Over the desert, dust is homogeneously mixed in the boundary layer (Carlson and Benjamin, 1980), which can be represented with a large value of σ_{height} such as 10. The optical depth τ_{550} measured by sun photometers reaches 2 near source regions (Moulin et al., 1997), but goes down to an average of 0.2–0.3 at Sal Island, which is situated downwind but close to the source region. To account for a continental region which would not be too specific of a dust storm situation, we chose the value 0.5. Over the eastern tropical Atlantic Ocean, the Saharan air layer is simulated with $\sigma_{\text{height}} = 2$, and $p_0 = 840$ hPa. The IPCC report gives a global value of 0.023 for dust optical depth, while Husar et al. (1997) measured an annual value of 0.2 above the West Atlantic, this value accounting for the whole aerosol burden. According to Moulin et al. (1997), an optical depth of 0.2 is more specific for regions closer to the source. For this study we chose the low value of 0.05 to account for a "background" dust downwind and far from the source. It is noticeable that the optical depth-forcing relationship is almost linear and well described (Coakley et al., 1983), and therefore the choice of a constant optical depth does not modify our conclusions.

One of the most important parameters to evaluate the radiative properties of dust is the complex refractive index, $m(\lambda) = n'(\lambda) - in''(\lambda)$, n' being the ratio of the light velocity in the medium to the light velocity in vacuum while n'' characterises the absorption of the medium. On the one hand, the real part n' is not thought to experience great variations with dust composition (Sokolik et al., 1993; Patterson, 1981), we therefore use $n'(\lambda)$ as described in Volz (1973) and Patterson (1981). On the other hand, the imaginary part n'' varies over a wide range as a function of the mineralogy. Since there are no complete measurements of $m(\lambda)$ throughout the spectrum, we define for the rest of the study three comprehensive cases representing realistic mineralogical compositions. For the remote oceanic case, where clay dominates (Volz, 1973), we use an index built on the Volz (1973)

and Patterson (1981) measurements from Barbados samples (hereafter "remote"). Such a composite refractive index has already been used in Tegen and Lacis (1996) and in d'Almeida (1987). For source regions, samples are supposed to contain more quartz (Lindberg and Gillepsie, 1977, Patterson, 1981), that sharpens and shifts the Si–O stretching vibration around 9.2 μm. Measurements on source region samples reproduce these features only for a limited wavelength range (Grams et al., 1974, Lindberg and Gillepsie, 1977), or do not show clearly these features (Sokolik et al., 1993). We use therefore in the desert case the composite refractive index (hereafter "source") of Ivlev and Popova (1973) linked in the visible to the 4 μm diameter category of Lindberg and Gillepsie (1977) and linked over 15 μm to the quartz results from Toon et al. (1977). For comparisons, we also use measurements of Sokolik et al. (1993) referred in the text as "source 2". The "remote", "source" and "source 2″ indices are presented over the whole spectrum in Fig. 2.

2.3. *Optical and radiative codes*

We calculate the radiative effect of mineral dust using the radiative code developed by Fouquart and Bonnel (1980) and Morcrette (1989) and presently used in the ECMWF forecast model. It uses a two stream formulation in the solar range with two spectral intervals (0.25–0.68 μm and 0.68–4.0 μm), and a broad band flux emissivity method in 6 spectral intervals between 0 and 2620 cm^{-1} in the infrared range. With the Delta-Eddington approximation, aerosol optical depth, τ_0, single scattering albedo, ω, and asymmetry parameter, g, are sufficient to compute the solar fluxes when combined with Rayleigh scattering and molecular absorption. The short-wave code has been compared with many others (Boucher et al., 1997), and is proven to overestimate, in absolute values, the positive and negative forcings of sulfate aerosols (between 10 and 20%). In the infrared spectrum, the atmosphere is assumed to be non-scattering and an optical depth is sufficient to describe aerosol effects. Aerosol optical parameters (Q_{ext}, ω, g) are calculated following Mie theory from *mnr*, σ_g, and $m(\lambda)$ under the assumption of a log-normal size distribution of homogeneous spherical particles. According to Mishchenko et al. (1995), non-sphericity of dust particles is not an issue for flux calculations. The parameters (Q_{ext}, ω, g) are spectrally averaged over all spectral intervals and tabulated for 9 values of the standard deviation and 64 values of *mnr*. Interpolation from the tabulated values of (Q_{ext}, ω, g) leads to maximum errors of 1%, which is satisfactory in view of the large saving of computing time that is achieved. Aerosol optical depth, τ_i, is evaluated in each spectral interval i from

$$\overline{\tau_i} \simeq \tau_{550} \frac{\overline{Q_{ext-i}}}{Q_{ext-550}}, \tag{3}$$

where τ_{550} is the optical depth at the 550 *nm* wavelength, $\overline{Q_{ext\text{-}i}}$ and $Q_{ext-550}$ are the extinction coefficient averaged over interval i and at 550 *nm*, respectively.

Forcings are integrated daily and yearly at the latitude 20°N where dust outbreaks occur above the Atlantic ocean. We compute the forcing for every 1° of solar zenith angle and make a weighted average to account for the diurnal and seasonal variations in solar zenith angle. Our forcings are therefore an annual mean except for the "winter" and "summer" forcing in Fig. 6 where forcings are computed for the winter and summer solstice respectively.

3. Forcing for the "ocean" and "desert" cases

Dust forcings for these 2 cases are presented in Table 3. The mineral dust effect is significant both for short-wave (SW) and long-wave (LW) radiation, at the top of the atmosphere (TOA) and at the surface.

At the surface, the net forcing is the result of short-wave loss of sunlight by absorption and back-scattering during the daytime, and of the permanent long-wave gain of energy by emission of dust. The surface forcing is therefore negative during the daytime and positive during the night. At the ocean surface, the SW reduction dominates and we find a yearly negative forcing. On the other hand, the desert case shows a positive forcing at the surface produced by the LW effect. The occurrence of this positive forcing is opposite to the conclusions of Sokolik and Golitsyn (1993) and to the common idea that aerosols always reduce energy fluxes at the surface. Since this feature depends mainly on the aerosol size distri-

Table 1. *Atmospheric, surface, and particle properties for the desert and the oceanic standard cases; references are given in the text*

Properties	Desert case	Oceanic case
Ground		
albedo R_s (SW)	0.3	0.06
surface mean temperature T_{surf} (°C)	27	24
surface diurnal temperature range ΔT° (°C)	30	0
Atmosphere		
temperature profile $T(z)$ (°C)	given in Fig. 1	given in Fig. 1
Particle properties		
mean number radius *mnr* (μm)	0.7	0.2
(i.e. mass median radius) (μm)	2.95	0.84
standard deviation σ_g	2.0	2.0
refractive index (imaginary)	"source"	"remote"
	given in Fig. 2 and Table 3	
Vertical distribution		
optical depth τ_0 at 550 nm	0.5	0.05
mean height p_0 (hPa)	840	840
height dispersion σ_{height}	mixed: 10	2

Table 2. *Spectrally weighted averages of the two refractive indices used in the two standard cases*

	Refractive index		
	imaginary part: n''		real part
	remote	source	
0.3–4 μm	6.57e-3	7.59e-3	1.534
4–100 μm	0.465	0.462	1.996
0.3–0.7 μm	6.66e-3	4.43e-3	1.562
0.7–2 μm	4.81e-3	9.36e-4	1.527
2–4.5 μm	1.01e-2	3.31e-2	1.482
4.5–8 μm	6.24e-2	0.141	1.414
8–12 μm	0.424	0.402	1.945
12–100 μm	0.564	0.552	2.134

Table 3. *Forcings in the 2 standard cases (Wm^{-2})*

TOA forcing			Surface forcing		
SW	LW	Net	SW	LW	Net
Ocean case					
−1.54	+0.15	−1.39	−3.89	+0.97	−2.92
Desert case					
+8.4	+11.9	+20.4	−33.3	+47.7	+14.4

bution for a fixed surface albedo, we will discuss it in details in Subsection 4.2.

With regard to the TOA, dust heats the Earth in trapping long-wave radiation ("greenhouse effect") while the short-wave effect is a negative forcing ("white-house effect", Schwartz, 1996) or a positive forcing depending on surface albedo and particle properties. In the oceanic standard case, we find a negative variation in the radiation budget at the TOA, which confirms the previous results of Carlson and Benjamin (1980). The desert case shows a strong positive forcing at the TOA. Tegen and Lacis (1996) found that large positive forcing above deserts compensate, on a global scale, the small negative forcing above oceans.

Measurements of dust forcings with the same surface and atmospheric parameters are seldom. Nevertheless, our results are qualitatively consistent with observations of Ackerman and Chung (1992) at the TOA and of Cautenet et al. (1992) at the surface.

4. Sensitivity to aerosol properties

4.1. The imaginary part of the refractive index n″

The imaginary part of the refractive index is known to have a large variability, essentially because dust is composed of particles of very

different mineralogy (Fig. 2, upper panel). Sokolik and Toon (1996) outlined its influence on radiative parameters but did not separate its effect from the size distribution effect. We want here to quantify the importance of the refractive index variability on forcing calculations independently from the size distribution.

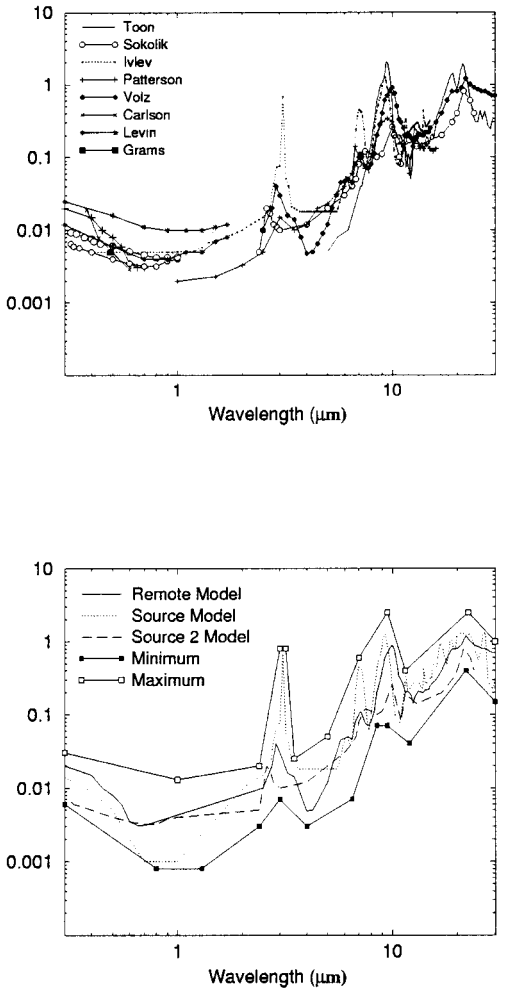

Fig. 2. Imaginary part of refractive indices. In the upper panel are shown existing measurements from Toon et al. (1977), Sokolik et al (1993), Ivlev and Popova (1973), Patterson (1981), Volz (1973), Carlson and Benjamin (1980), Levin et al. (1979), Grams et al. (1974) and Lindberg and Gillepsie (1977). In the lower panel are presented the composite refractive indices defined in the text, and the maximum and minimum envelope also used in this study.

The absolute variability of the imaginary part $n''(\lambda)$ is reflected in the "maximum" and "minimum" envelope of known refractive indices (Fig. 2, lower panel). Using these two indices, the standard cases shows large differences in the obtained dust forcing: for instance at the TOA in the ocean case, the "maximum" envelope is responsible for a large SW absorption ($+0.95$ W m^{-2}) and therefore for a net positive forcing (1.16 W m^{-2}), contrary to the standard case (-1.39 W m^{-2}). In the same way, in the desert case, the net SW surface forcing goes down to -60 W m^{-2} with the "maximum" envelope, which represents a 100% difference to the standard case. The refractive index absolute variability is therefore responsible for an uncertainty on the amplitude and on the sign of desert dust radiative forcings. In order to reduce these uncertainties, we focus in the following on two major sources of variability: differences in the mineralogical composition of dust samples, but also large uncertainties (40%) in refractive index measurements (Patterson, 1981; Sokolik et al., 1993).

The variability with the mineralogy of the imaginary part $n''(\lambda)$ is reflected in the "remote", "source" and "source 2" indices defined previously as representative cases of real mineralogical situations, we therefore apply them to the standard cases (Table 4, first lines). It is noteworthy that these two new cases are not unrealistic: a "remote" dust model can occur above a continent far from the sources (e.g., above Europe) and a "source" mineral aerosol could be observed above the east Atlantic during large dust outbreaks. This variability in the mineralogy is responsible for an uncertainty between ± 11 and ± 16% at the TOA and between ± 8 and ± 40% at the surface (Table 4). For instance, the "remote" clay-rich absorbs more solar energy than the "source" quartz-rich samples because n'' is higher in this range. This can be seen above the desert where the TOA forcing increases by 7.7 W m^{-2} (from 20.4 to 28.1 W m^{-2}), when we apply the "remote" dust composition.

Measurements on the imaginary part of refractive index are known to have an uncertainty of 40% (Patterson, 1981, Sokolik et al., 1998). Since we do not know how this error is distributed with wavelength, we chose to make a maximum assumption and raised or reduced the refractive index linearly by 40% throughout the spectrum. When we apply these indices, variations in forcing

Table 4. *Optical factors contributing to the uncertainties in calculations of dust radiative effect*

Factors contributing to uncertainty	Top of the atmosphere forcing range ($W\,m^{-2}$)	Top of the atmosphere Δ	Surface forcing range ($W\,m^{-2}$)	Surface Δ
		ocean case		
refractive indices				
mineralogical variability	−1.39: −1.72	±11%	−2.49: −2.92	±8%
measurements variability	−1.20: −1.72	±17%	−2.77: −3.07	±4%
size distribution				
numerical treatments	−1.14: −1.39	±10%	−2.51: −2.81	±5%
		desert case		
refractive indices				
mineralogical variability	20.4: 28.1	±16%	6.2: 14.4	±40%
measurements variability	14.8: 24.6	±25%	13.5: 16.2	±9%
size distribution				
numerical treatments	20.2: 20.9	±1.5%	14.4: 15.2	±2.5%

Net forcings at the surface and at the top of the atmosphere are ranked and an uncertainty factor is given for each parameter. We test the mineralogical variability of the refractive index with the "source", "source2" and "remote" indices defined in the text, and the variability in indices measurements is tested by rising or reducing the indices from 40% throughout the spectrum. For the size distribution, a gamma, a log-normal and a "bins" numerical treatments are used.

are around ±20% at the TOA and are under ±10% at the surface.

From these 2 experiments, the variability in forcing calculations due to the only refractive index variability reaches ±40% at the TOA. This point brings 2 conclusions: first extensive measurements of the dust refractive indices with reduced uncertainties are necessary, and second a mineralogical understanding and modelling of dust outbreaks should be developed since the use of one refractive index for all situations lead to large uncertainties. On the other hand, the mineralogical modelling of desert dust is probably very difficult since it requires a knowledge of sources, transport, mixing and refractive index of all species.

Nevertheless, the calculation would be easier if the wavelength dependence of $n''(\lambda)$ could be neglected, i.e., if the averaging of $n''(\lambda)$ and of the optical parameters over the wavelength spectrum would eliminate the non linearity of the Mie calculations. This would reduce the number of variables and allow comparisons with measurements which are often limited or integrated on a spectral band. Such a discretisation of the refractive index was used by Carlson and Benjamin (1980) who chose 13 intervals. To go further, we test here two cases: a two interval weighted average (visible and infrared), since such indices are sometimes used, and a six interval weighted average. The latter discretisation was chosen to catch mineralogical variability: 0.3–0.7 μm for the visible, 0.7–2 μm for the near infrared which is seldom measured, 2–4.5 μm for the 3 μm absorption peak (quartz, sulfates, water, etc), 4.5–8 μm for the 7 μm carbonate peak, 8–12 μm for the silicate signature and 12–100 μm for the far infrared. Averages of the refractive indices are shown in Table 2. In the ocean case, the two averaging method are satisfactory with variations within 6% compared to the reference case, whereas the desert case is poorly represented even with the six intervals scheme, with variations with the reference case up to 32%. This difference is explained by the internal variability of the refractive indices: the "source" index is very variable, with changes of orders of magnitude along the spectrum. Such variations bring important non-linearities inside Mie calculations. These tests clearly show that the whole wavelength dependency needs to be considered.

4.2. *Sensitivity to aerosol size distribution*

In order to calculate optical properties, the population of particles can be described by the

two first moments of its size distribution (Hansen and Travis, 1974). We focus here on the mean number radius *mnr* and on the geometric standard deviation σ_g, and show how they influence dust radiative impact. Then we outline the ability of the different size distribution schemes used in global models to reproduce the optical properties of the two standard cases.

It is important to emphasise that our study is made with a constant optical depth and not for a constant aerosol mass loading: when the *nmr* rises the total mass rises too. This approach is justified because satellite measurements provide a constraint on aerosol optical depth. The variations of radiative parameters as a function of the mean radius for different σ_g are shown in Fig. 3.

4.2.1. Sensitivity to the mean number radius mnr. The importance of *mnr* on the radiative parameters is evident from Fig. 3, upper panel. With a greater *mnr*, the visible absorption and forward scattering increase, but also the extinction ratio $\overline{Q_{\text{ext}-\text{IR}}}/Q_{\text{ext}-550}$. The latter implies that the LW forcing takes more importance when large particles are included in the size spectrum. The influences of these variations on radiative forcings are presented in Fig. 4 where we vary *mnr* based on the two standard cases, the standard deviation of the size distribution being fixed to the reference value of 2.

At the top of the atmosphere (Fig. 4, upper panels), the long-wave forcing is positive and the short-wave forcing is negative for small, backscattering, particles and positive for large, absorbing, particles. These two components are both slowly increasing with the *mnr* for small distributions and steeply increasing when *mnr* is over 0.3 μm (*mmr* above 2.1 μm). As a result, a 20% uncertainty in the *mnr* is responsible for a negligible variation (under 1%) in the forcing calculation above the ocean, where $mnr = 0.2\mu m$, and for a 22% uncertainty in the forcing calculation above the desert where $mnr = 0.7\mu m$. One should also notice that the net TOA forcing turns from a negative to a positive value for a *mnr* around 0.5 μm above the ocean ($mmr = 2.1$ μm), and for *mnr* around 0.2 above the desert ($mnr = 0.84$ μm). The change of the TOA forcing from positive to negative is an important feature that we discuss in Section 5 together with the surface albedo dependence of the forcing.

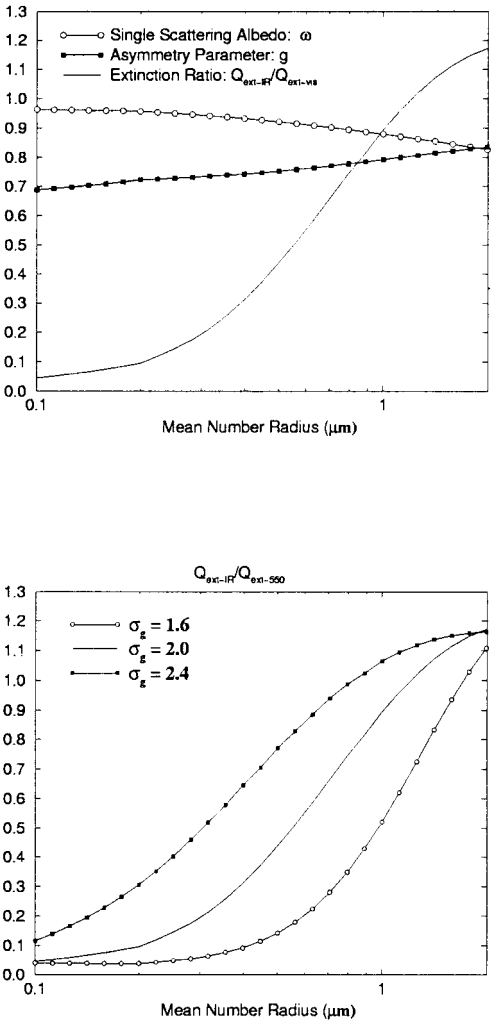

Fig. 3. Single scattering albedo, ω, and asymmetry parameter, g, in the visible range as a function of mean number radius (μm). Also shown is the ratio of the extinction efficiency in the infrared to that at 550 nm, $Q_{\text{ext}-\text{IR}}/Q_{\text{ext}-550}$. In the upper panel, results are given for a geometric standard deviation of the size distribution $\sigma_g = 2$. In the lower panel, results for $Q_{\text{ext}-\text{IR}}/Q_{\text{est}-550}$ are given for 3 different values of σ_g (1.6, 2 and 2.4). The refractive index is the "remote" one (see text and Fig. 2).

At the surface (Fig. 4, lower panels), the LW positive forcing is opposite to the SW forcing. With increasing *mnr*, the larger absorption (LW and SW) in the dust layer is responsible for a positive LW forcing and a negative SW forcing. Nevertheless the LW effect increases more steeply

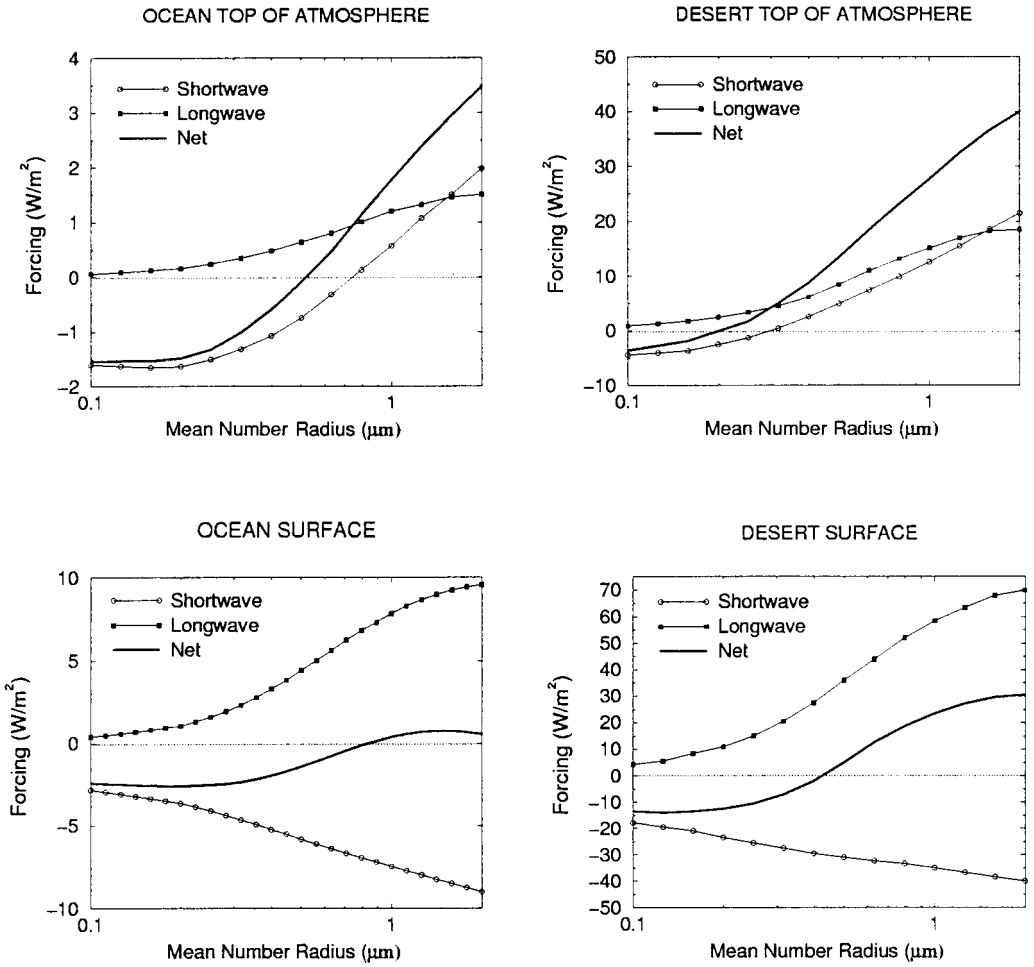

Fig. 4. Mineral dust forcing (short-wave, long-wave, and net in W m^{-2}) at the TOA (upper panels) and at the surface (lower panels) as a function of mean number radius, mnr. The results are presented for the oceanic case (left panels, $\tau = 0.05$) and the desert case (right panels, $\tau = 0.5$), the geometric standard deviation of the size distribution is $\sigma_g = 2.$ in both cases. Note the different scales for the forcings.

and the net radiative budget at the ground rises with *mnr* from negative values over the ocean to significant positive values over the desert. As previously at the TOA, surface forcings are much more sensitive to the *mnr* when large particles are involved (large *mnr*). To understand how such a positive forcing can occur at the desert surface, the determinant parameter is $\overline{Q_{\text{ext}-\text{IR}}}/Q_{\text{ext}-550}$, hereafter *k*. Measurements of *k* made in Tadzhikistan during the USSR-USA campaign gave values between 0.3 and 0.5 (Sokolik and Golitsyn, 1993) and d'Almeida (1987) found a *k* close to 0.55 in the Sahara, all these values being representative of a dust "background" loading. In our desert case, *k* is equal to 0.6 because we study here a pure dust cloud. One should note that Fouquart et al. (1980) and Carlson and Benjamin (1980) estimated *k* between 0.1 and 0.3 but with smaller *mnr*. In fact, the relationship between *mnr* and *k* is very sensitive when *mnr* is larger than 0.3 μm (*mmr* = 1.26 μm) (see Fig. 3): for example, *k* = *0.3* corresponds to a *mnr* close to 0.35 μm (*mmr* = 1.48 μm, desert "background") while *k* = *0.55* corresponds to a *mnr* equal to 0.6 μm (*mmr* =

2.5 μm, dust outbreak). In their one dimension study, Sokolik and Golitsyn (1993) resorted to use $k=0.3$ and concluded then to a systematic negative forcing at the surface. This result is also shown on Fig. 4: forcing at the surface are negative when *mnr* is under 0.41 μm ($mmr=1.72$ μm), but a significant gain of energy also appears at the ground for larger *mnr*, i.e., in dust storm conditions, and since these events are probably responsible for a large dynamic response, such a result is noteworthy.

4.2.2. Sensitivity to the standard deviation σ_g of the size distribution. If we go back to Fig. 3, lower panel, we see that the standard deviation σ_g of the size distribution has a strong effect on the extinction ratio $\overline{Q_{ext-IR}}/Q_{ext-550}$. The effect of σ_g on parameters in the visible (g and ω) is small and not shown. An increase in σ_g brings large particles in the size distribution. Their large surface, together with a large extinction coefficient, is responsible for an increase of Q_{ext-IR} (and a decrease of ω), and therefore of τ_{IR}/τ_{550}. The influence of σ_g is then the composition of a growing LW influence and, to a smaller extent, of a larger SW absorption. As reflected in Fig. 5, results are mainly an increase in forcings at the surface and at the TOA, both for the desert and oceanic cases. The quasi-linearity and the low sensitivity of the σ_g-forcing relationship around $\sigma_g=2$ is noteworthy: if σ_g remains close to 2 (d'Almeida, 1987), the use of an average value for σ_g is sufficient. Only for large variations of σ_g, effects on the visible radiative parameters bring noticeable non-linearities (Fig. 5). For example, with a $\sigma_g=3.2$ (Shettle, 1984) the TOA forcing above the desert increases by more than 20 W m^{-2}. But such a large σ_g is seldom observed.

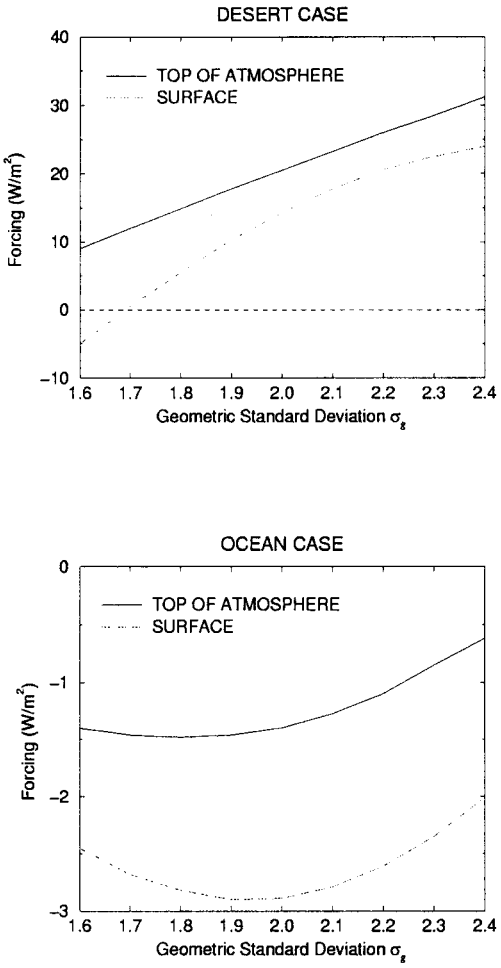

Fig. 5. Net dust forcing (W m^{-2}) at TOA and at the surface as a function of the geometric standard deviation σ_g of the size distribution. Results are for the desert case (left panel) and the oceanic case (right panel) as defined in Tables 1, 2. Mean number radius is 0.7 and 0.2 μm, respectively.

4.3. *Sensitivity to the numerical treatment of the size distribution*

One can handle the aerosol size distribution by two numerical treatments: a "bin" scheme, where particles are distributed into size classes which are then used as tracers, and a "spectral" scheme where the evolution of the population is described by the variation of its first moments (e.g., the mean mass diameter and the standard deviation) assuming any regular type of distribution. The assumption of constant optical properties in each bin for the first case and the arbitrate choice of shape for the distribution for the second case are both responsible for uncertainties in the calculations. We aim to assess here if these uncertainties are significant for radiative calculations. The quality of spectral scheme representation in transport models has been discussed in Schulz et al. (1998).

The application of a "bin" scheme to dust radiative calculations has been initiated by Tegen and Lacis (1996). Each of their 8 bins has constant

optical properties assuming for each bin a gamma distribution with $\sigma_{\text{eff}} = 0.2$, σ_{eff} being the effective standard deviation. That means that radiative parameters are fixed for each bin and used after transport to evaluate properties for the whole population. We applied this approach to the two standard cases in redistributing the log-normal distribution in the eight bins defined in Tegen and Lacis (1996), spanning from 0.1 to 10 μm. Both in the desert and in the ocean case, results are very close (within 10%) to the calculations with the log-normal distribution (Table 4).

On the other hand, if one would use a spectral representation of the size distribution, one would need to decide the shape of its size distribution. To test the importance of this choice, we applied gamma distributions to our standard cases, keeping constant the effective radius and effective variance (Hansen and Travis, 1974) and we observe the difference with log-normal distributions used previously. There are no significant differences between these numerical treatments of the size distribution (Table 4). Nevertheless, for the ocean case, where the SW forcing dominates, a large part of the variability is explained by differences in the LW forcing which goes from 0.15 to 0.20 W m^{-2} with the gamma distribution, especially because of differences in the treatment of small particles. This finding temperates the conventional view that the effective radius and effective radiance of an aerosol population are sufficient to predict the aerosol optical properties.

5. Sensitivity to column and surface properties

In this section, we focus on the column properties, i.e. the distribution of temperature and dust with height, but also LW emissivity and SW albedo.

5.1. *Sensitivity to the column distribution*

In our model, the temperature profile is determined by three parameters: the surface daily-averaged temperature, T_{surf}, its diurnal amplitude, ΔT_{surf}, and the shape of the vertical temperature profile. The surface temperature influences the whole boundary layer following a given profile which decreases with height for the desert case and includes a temperature inversion between 980 and 900 hPa for the oceanic case. The influence of temperature profile on forcing is closely linked to dust distribution with height because these two profiles both act on LW fluxes. Note that the dust forcing at the TOA depends on the difference between the ground temperature and the aerosol temperature while the surface forcing depends on the aerosol layer temperature. In this section, we will often consider the energy deposition in the dust layer (net forcing at the TOA − net forcing at the surface). This deposition is necessary to evaluate any atmospheric response to a forcing and depends on the column distribution of temperature and dust. One should note that this energy deposition is around 1.5 W m^{-2} in the ocean case and 6 W m^{-2} in the desert case.

The TOA forcing increases with the surface mean temperature $\overline{T}_{\text{surf}}$ since LW fluxes are linked to $\overline{T^4}_{\text{surf}}$. In fact, $\overline{T}_{\text{surf}}$ controls also the temperature in the dust layer, therefore, the surface forcing increases with $\overline{T}_{\text{surf}}$. But even for the desert case where surface temperature are subject to large variations, a 5°C error in $\overline{T}_{\text{surf}}$ only leads to a 2 W m^{-2} in the TOA forcing and 3 W m^{-2} at the surface. Therefore, since surface temperatures are usually well known, they should not be responsible for large errors in dust forcing calculations. However, one has to remember that a dust cloud influences the soil temperature (Cautenet et al., 1992), and that the occurrence of a positive feedback is therefore possible.

The dust height at mean pressure level p_0 determines the temperature of the dust layer. The higher the dust layer is, the larger the TOA forcing is and the smaller the surface forcing: a high layer traps more energy in the dust cloud. In the ocean case, if the mean height of the dust layer goes from 926 to 717 hPa, the energy kept in the atmosphere raises from nearly from 1.5 to 2.5 W m^{-2} (60% difference). This points out that the evaluation of a climatic impact of dust may need a precise knowledge of its vertical distribution.

The shape of the temperature profile and σ_{height}, i.e. the "physical" depth of the dust cloud, act together on the dust radiative forcing because they influence the dust layer mean temperature. For example above the desert, if σ_{height} goes from 10 to 2 (Fig. 1), the dust height being constant, the energy deposition in the dust layer raises from 6

to 8 W m^{-2} (+33%). This proves that the surface negative forcing of high dust is not completely compensated by the positive forcing of low dust, therefore the average height of the dust layer is not enough to assess its LW effect. The non-validity of an "average height" in radiative calculation is noticeable for mineral dust which is often distributed in many thin layers (Swap et al., 1992).

The diurnal temperature range does not play a significant role. The daytime high LW forcing compensates for the nighttime low LW forcing. If we neglect a possible dynamic effect, a daily average of the temperature is enough to evaluate a radiative forcing.

5.2. *Sensitivity to surface LW emissivity and SW albedo*

Following Legrand et al. (1992), the LW emissivity of the surface emissivity ε varies in the desert between 0.9 and 1. Applying $\varepsilon = 0.9$ in the desert case reduces the TOA by 2 W m^{-2} and the surface forcing by 5 W m^{-2}. Since ε acts linearly on the emission of LW radiation by the ground, it also has a linear impact on the forcing, therefore averages are sufficient for global calculations.

The SW forcing is known to increase linearly with $(1-R_s)^2$ (Charlson, 1992), but only for R_s under 0.4 (Boucher et al., 1997). At the top of the atmosphere, the dust forcing evolves with this albedo from negative values over oceans to positive values over highly reflecting surfaces (e.g, ice sheets or clouds). But the sign of the TOA forcing also depends on the solar zenith angle (Weare et al., 1974, Haywood and Shine,1995), and on the dust vertical distribution (Tegen and Lacis, 1996). Sokolik and Toon (1996) also noticed the importance of the "aerosol model" to determine the sign of the forcing but did not separate the size distribution effect from the refractive index effect. In Fig. 6, we compare the importance of all these parameters and it appears that the refractive has a large impact on the sign of the TOA forcing independently from the *mnr*. Tegen and Lacis (1996) found that the sign of the TOA forcing changes for a critical *mnr*, hereafter mnr_c, equal to 0.54 μm (after conversion from the effective radius to the mean number radius) for a dust cloud between 0 and 3000 m. Their results are hardly comparable to ours since they use a modelled distribution, nevertheless, if we focus on $R_s = 0.15$,

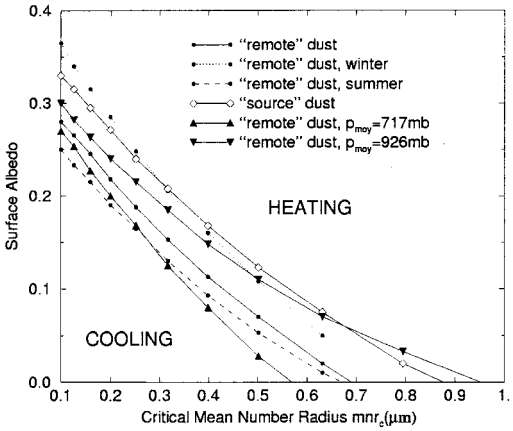

Fig. 6. Regions of net positive/negative forcing at the TOA as a function of the surface albedo, R_s, and the mean number radius, *mnr*. In the region of the graph above each curve, the dust heats the Earth/Atmosphere system, while under each curve the system is cooled. Results are presented for two refractive indices (clay rich: "remote", and clay and quartz: £source"), and then with the "remote" dust for two seasonal extrema (winter and summer solstice) and for two different heights of the dust layer (p_0 of 926 and 717 hPa). We use the parameters of the oceanic case defined in Table 1 except for the mean number radius and surface albedo which are varied between 0.1 to 1.μm and 0 to 0.4, respectively.

close to the mean global albedo, it appears in Fig. 6 that mnr_c is always under 0.45 μm. This difference is mainly due to the vertical distribution: with a dust cloud extending up 3600, the mnr_c is between 0.35 and 0.52 μm. One should also notice that a $R_s = 0.15$ also corresponds to a "dark continent" situation. In such a region, e.g in Asia, where data on the vertical distribution and on the dust mineralogy are sparse, it is therefore very difficult to determine the sign of the TOA dust forcing. These experiments shows that the refractive index and the vertical distribution of the dust are the most sensitive parameters for the determination of a dust radiative effect.

6. Conclusion

A sensitivity study on the net climate forcing by mineral dust in clear sky conditions has been developed with a single-column model to determine how various parameters have to be taken into account in a global approach. Two standard

cases (desert and ocean) are assumed to account for a significant fraction of the variability found over the North African-Atlantic region where globally most of the dust loading occurs. Both the short-wave and the long-wave contributions are studied, the latter being found to be never negligible because of the large LW absorption of desert dust.

We can summarise our conclusions in three points: first, the refractive index appears to be a critical parameter in determining a global effect as expected from the study by Sokolik and Toon (1996). The largest uncertainty comes from the mineralogical variability of dust samples: in the desert case, between two realistic indices for mineral dust, forcings exhibit a $\pm 16\%$ variation at the TOA and $\pm 40\%$ at the surface. This refractive index has a large variability with the wavelength and averaging it brings large errors in radiative fluxes calculations. Since the mineralogy changes with sources and during the transport, one of the challenging problem for radiative calculations will therefore be to model dynamically this complex refractive index. Besides, index measurements are old and imprecise, reaching a 40% uncertainty. This is responsible for a $\pm 25\%$ uncertainty in the desert TOA radiative fluxes determination. Secondly, the importance of the long-wave component in the net forcing gives a large influence to the vertical distribution of dust, and, to a smaller extend, to the vertical profile of temperatures. As described by Tegen et Lacis (1996), this has a crucial effect of the sign of the TOA forcing, but it also determines the amplitude of the energy deposition inside the dust layer which may control the dynamic response. Third, the knowledge of the mean radius of the size distribution is needed to determine the amplitude of forcings when large particles are involved. In contrast, assumptions made for numerical treatments of the size distribution ("bins", log-normal, gamma distribution) do not introduce significant uncertainties in respect to radiative calculations.

The aim of our study was not to describe the forcing on a global scale, but rather to document two standard cases that are representative of dust occurrence. For instance, above the ocean, net radiative fluxes are reduced at the top of the atmosphere and at the surface, leading to a global cooling. On the other hand above the desert, the forcing exceeds frequently $+ 24$ to $28\ \mathrm{W\,m^{-2}}$ at the top of the atmosphere with a high energy deposition in the aerosol layer, while the surface gains energy because of the LW effect. This implies that the boundary layer stability could be modified by such a dust layer and underscores the possibility of a large local dynamical response.

7. Acknowledgement

This work would not have been possible without the radiative code provided and explained by Jean-Jacques Morcrette. Our money support came from the German-French cooperation fund PROCOPE, the EU-ENVIRONMENT AND CLIMATE project SINDICATE (contract EV5V–CT92–122) and project MEDUSE (contract ENV4–CT95–0036) both supported by the European Commission (DG XII). This is the LSCE contribution number 69.

REFERENCES

Ackerman, S. and Chung, H. 1992. Radiative effect of airborne dust on regional energy budgets at the top of the atmosphere. *J. Appl. Meteo.* **31**, 223–233.

Boucher, O. and Anderson, T. L. 1995. GCM assessment of the sensitivity of direct climate forcing by anthropogenic sulfate aerosols to aerosol size and chemistry. *J. Geophys. Res.* **100**, 26117–26134.

Boucher, O., Schwartz, S. E., Ackerman, T. P., Anderson, T. L., Bergstrom, B., Bonnel, B., Chýlek, P., Dahlback, A., Fouquart, Y., Fu, Q., Halthore, R. N., Haywood, J. M., Iversen., T., Kato, S., Kinne, S., Kirkevåg, A., Knapp, E., Lacis, A., Laszlo, I., Mishchenko, M. I., Nemesure, S., Ramaswamy, V., Roberts, D. L., Russel, P., Schlesinger, M. E., Stephens, G. L., Wagener, R., Wang, M., Wong, J. and Yang, F. 1998. Intercomparison of models representing short-wave radiative forcing by sulfate aerosols. *J. Geophys. Res.*, in press.

Cabot, F. 1995. *Estimation de l'albédo de surface à l'échelle globale à l'aide de mesures satellitaires*. Thèse d'université, Université d'Orsay Paris Sud.

Carlson, T. B. and Benjamin, S. G. 1980. Radiative heating rates for Sahara dust. *J. Atmos. Sci.* **37**, 193–213.

Cautenet, G., Legrand, M., Cautenet, S., Bonnel, B. and Brogniez, G. 1992. Thermal impact of Saharan dust over land. Part I: simulation. *J. Appl. Meteo.* **31**, 166–180.

Charlson, R. J., Schwartz, S. E., Hales, J. M., Cess, R. D., Coakley, J. A., Hansen, J. E. and Hofmann, D. J. 1992.

Climate forcing by anthropogenic aerosols. *Science* **255**, 423–430.

Coakley, J. A., Cess, R. D. and Yurevich, F. B. 1983. The effect of tropospheric aerosols on the Earth's radiation budget. A parameterization for climate models. *J. Atmos. Sci.* **40**, 116–138.

D'Almeida, G. A. 1987. On the variability of desert aerosol radiative characteristics. *J. Geophys. Res* **92**, 3017–3026.

Dulac, F., Tanré, D., Bergametti, G., Buat-Ménard, P., Desbois, M. and Sutton, D. 1992. Assessment of the African airborne dust mass over the Western Mediterranean Sea using Meteosat data. *J. Geophys. Res.* **97**, 2489–2506.

Fouquart, Y. and Bonnel, B. 1980. Computations of solar heating of the Earth's atmosphere. A new parameterization. *Beitr. Phys. Atmos.* **53**, 35–62.

Fouquart, Y., Bonnel, B., Roquai, M. C., Santer, R. and Cerf, A. 1987. Observations of Saharan aerosols. Results of ECLATS field experiment. Part I. Optical thicknesses and aerosol size distributions. *J. Clim. Appli. Meteor*. **26**, 28–37.

Gomes, L., Bergametti, G., Coudé-Gaussen, G. and Rognon, P. 1990. Submicron desert dusts. A sandblasting process. *J. Geophys. Res* **95**, 13929–13935.

Grams, G. W., Blifford, I. H., Gillette, D. A. and Russel, P. B. 1974. Complex index of refraction of airborne soil particles. *J. Appl. Meteo.* **13**, 459–471.

Hansen, J. E. and Travis, L. D. 1974. Light scattering in planetary atmospheres. *Space Sci. Rev.* **16**, 527–610.

Haywood, J. M. and Shine, K. P. 1995. The effect of anthropogenic sulphate and soot aerosol on the clear sky radiation budget. *Geophys. Res. Lett*. **22**, 603–606.

Husar, R. B., Prospero, J. M. and Stowe, J. M. 1997. Characterization of the tropospheric aerosols over the oceans with the NOAA Advanced Very High Radiometer optcial thickness operational product. *J. Geophys. Res.* **102**, 16889–16910.

IPCC1995. *Summary for policymakers*. Cambridge University Press.

Ivlev, L. S. and Popova, S. I. 1973. The complex refractive indices of substances in the atmospheric-aerosol dispersed phase. *Izv. Atmosph. and Ocean. Phys.* **10**, 1034–1043.

Kiehl, J. T. and Briegleb, B. P. 1993. The relative role of sulfate aerosols and greenhouse gases in climate forcing. *Science* **260**, 311–314.

Legrand, M., Cautenet, G. and Buriez, J. C. 1992. Thermal impact of Saharan dust over land. Part II. Application to satellite IR remote sensing. *J. Appl. Met*. **31**, 181–193.

Levin, Z. and Lindberg, J. D. 1979. Size distribution, chemical composition and optical properties of urban and desert aerosols in Israel. *J. Geophys. Res.* **84**, 6941–6950.

Linberg, J. D. and Gillepsie, J. B. 1977. Relationship between particle size and imaginary refractive index in atmospheric dust. *Appl. Optics* **16**, 2628–2630.

Mishchenko, M. I., Lacis, A. A., Carlson, B. E. and Travis, L. D. 1995. Non-sphericity of dust like tropospheric aerosol. Implications for aerosol remote sensing and climate modelling. *Geophys. Res. Lett*. **22**, 1077–1080.

Morcrette, J. J. 1989. *Technical memorandum 165: Description of the radiation scheme in the ECMWF model*. ECMWF, Reading, U.K.

Moulin, C., Dulac, F., Lambert, C. E., Chazette, P., Jankowiak, I., Chatenet, B. and Lavenu, F. 1997. Long term daily monitoring of Saharan dust load over marine areas using meteosat ISCCP-B2 data (2). Accuracy of the method and validation using sun photometers measurements. *J. Geophys. Res.* **102**, 16959–16968.

Patterson, E. M. 1981. Optical properties of the crustal aerosol. Relation to chemical and physical characteristics. *J. Geophys. Res.* **86**, 3236–3236.

Payne, R. E. 1972. Albedo of the sea surface. *J. Atmos. Sci.* **29**, 959–970.

Penner, J. E., Dickinson, R. E. and O'Neill, C. A. 1992. Effects of aerosol from biomass burning on the global radiation budget. *Science* **256**, 1432–1434.

Riehl, H. 1954. *Tropical meteorology*. McGraw-Hill.

Schulz, M., Balkanski, Y., Dulac, F. and Guelle, W. 1998. Treatment of aerosol size distribution in a global transport model: validation with satellite-derived observations for a Saharan dust episode. *J. Geophys. Res.* **103**, 10579–10592.

Schütz, L. 1979. Sahara dust transport over the North Atlantic Ocean. Model calculations and measurements. In: *Saharan dust*, pp. 267–277. John Wiley.

Schütz, L. 1980. Long range transport of desert dust with special emphasis on the sahara. *Ann. N. Y. Acad. Sci.* **338**, 15–20.

Schwartz, S. E. 1996. The whitehouse effect. Shortwave radiative forcing of climate by anthropogenic aerosols. An overview. *J. Aer. Sci.* **27**, 359–382.

Shettle, E. P. 1984. Optical and radiative properties of a desert aerosol model. In *Proceedings of the Symposium on Radiation in the atmosphere, edited by G. Fiocco*, pp. 74–77. A. Deepak, Hampton, Va.

Sokolik, I., Andronova, A. and Johnson, T. C. 1993. Complex refractive index of atmospheric dust aerosols. *Atmos. Env.* **27A**, 2495–2502.

Sokolik, I. and Golitsyn, G. 1993. Investigation of optical and radiative properties of atmospheric dust aerosols. *Atmos. Env.* **27A**, 2509–2517.

Sokolik, I. N. and Toon, O. B. 1996. Direct radiative forcing by anthropogenic airborne mineral aerosol. *Nature* **381**, 681–683.

Sokolik, I. N., Toon, O. B. and Bergström, R. W. (1998). Modeling the radiative characteristics of airborne mineral aerosols at infrared wavelength. *J. Geophys. Res.* **103**, 8813–8826.

Swap, R., Garstang, M., Greco, S., Talbot, R. and Gac, J. Y. 1992. Sahara dust in the Amazon bassin. *Tellus* **44B**, 133–149.

Tanré, D., Devaux, C., Herman, M., Santer, R. and Gac,

J. Y.1988. Radiative properties of desert aerosols by optical ground based measurements at solar wavelengths. *J. Geophys. Res.* **93**, 14223–14231.

Tegen, I. and Lacis, A. A. 1996. Modeling of particle size distribution and its influence on the radiative properties of mineral dust aerosol. *J. Geophys. Res.* **101**, 19237–19244.

Tegen, I., Lacis, A. A. and Fung, I. 1996. The influence of mineral aerosols from disturbed soils on the global radiation budget. *Nature* **380**, 419–422.

Toon, O. B., Pollack, J. B. and Sagan, C. 1977. Physical properties of the particles composing the martian dust storm of 1971–1972. *Icarus* **30**, 663–696.

Twomey, S. A., Piepgrass, M. and Wolfe, T. 1984. An assessment of the impact of pollution on global cloud albedo. *Tellus* **36B**, 243–249.

Volz, F. E. 1973. Infrared optical constants of ammonium sulfate, Sahara dust, volcanic pumice and flyash. *Appl. Optics* **12**, 564–568.

Weare, B. C., Temkis, R. L. and Snell, F. M. 1974. Aerosol and climate: some further modifications. *Science* **186**, 827–828.